The Journal of Chemical Physics

# Extension of natural reaction orbital approach to multiconfigurational wavefunctions

Cite as: J. Chem. Phys. **157**, 084118 (2022); https://doi.org/10.1063/5.0098230
Submitted: 06 May 2022 • Accepted: 01 August 2022 • Accepted Manuscript Online: 05 August 2022 • Published Online: 25 August 2022

**Shuichi Ebisawa, Takuro Tsutsumi and Tetsuya Taketsugu**



AIP Publishing

The Journal of Chemical Physics ARTICLE scitation.org/journal/jcp

# Extension of natural reaction orbital approach to multiconfigurational wavefunctions

Cite as: J. Chem. Phys. **157**, 084118 (2022); doi: 10.1063/5.0098230
Submitted: 6 May 2022 • Accepted: 1 August 2022 •
Published Online: 25 August 2022



Shuichi Ebisawa,[1] Takuro Tsutsumi,[2,3] and Tetsuya Taketsugu[2,4,a)]

## AFFILIATIONS

[1] Graduate School of Chemical Sciences and Engineering, Hokkaido University, Sapporo 060-0810, Japan
[2] Department of Chemistry, Faculty of Science, Hokkaido University, Sapporo 060-0810, Japan
[3] L-Station, Creative Research Institution (CRI), Hokkaido University, Sapporo 060-0812, Japan
[4] Institute for Chemical Reaction Design and Discovery (WPI-ICReDD), Hokkaido University, Sapporo 001-0021, Japan

**Note:** This paper is part of the JCP Special Topic on Nature of the Chemical Bond.
[a)] **Author to whom correspondence should be addressed:** take@sci.hokudai.ac.jp

## ABSTRACT

Recently, we proposed a new orbital analysis method, natural reaction orbital (NRO), which automatically extracts orbital pairs that characterize electron transfer in reaction processes by singular value decomposition of the first-order orbital response matrix to the nuclear coordinate displacements [Ebisawa *et al.*, Phys. Chem. Chem. Phys. **24**, 3532 (2022)]. NRO analysis along the intrinsic reaction coordinate (IRC) for several typical chemical reactions demonstrated that electron transfer occurs mainly in the vicinity of transition states and in regions where the energy profile along the IRC shows shoulder features, allowing the reaction mechanism to be explained in terms of electron motion. However, its application has been limited to single configuration theories such as Hartree–Fock theory and density functional theory. In this work, the concept of NRO is extended to multiconfigurational wavefunctions and formulated as the multiconfiguration NRO (MC-NRO). The MC-NRO method is applicable to various types of electronic structure theories, including multiconfigurational theory and linear response theory, and is expected to be a practical tool for extracting the essential qualitative features of a broad range of chemical reactions, including covalent bond dissociation and chemical reactions in electronically excited states. In this paper, we calculate the IRC for five basic chemical reaction processes at the level of the complete active space self-consistent field theory and discuss the phenomenon of electron transfer by performing MC-NRO analysis along each IRC. Finally, issues and future prospects of the MC-NRO method are discussed.



## I. INTRODUCTION

As is well known, molecular orbitals (MOs)[1,2] are very useful in understanding the reactivity of chemical reactions. Fukui's frontier orbital theory[3,4] and the Woodward–Hoffmann rule[5–9] are the most representative works that reveal the essence of chemical reactivity in terms of MOs. These two theories have been widely accepted and applied to various systems involving reactions in electronically excited states. Although frontier orbital theory and the Woodward–Hoffmann rule were established more than half a century ago, the concept of MO is by no means old. In recent years, properties of MOs, such as orbital energies, have been used as descriptors in cutting-edge data science approaches.[10,11] Molecular orbitals are still a powerful tool for extracting the essence of chemical phenomena, a concept with such a long history that it still underlies chemists' thinking today. However, it is not clear whether the properties of MOs are fully exploited in the analysis of reaction mechanisms.

In standard reaction mechanism analysis, the interaction of MOs possibly involved in a chemical reaction is traced along reaction coordinates.[8] Therefore, MOs and reaction coordinates that characterize a reaction are necessary to perform reaction mechanism analysis. Nowadays, with the development of computational chemistry, it is easy to obtain MOs for molecular systems, and various sophisticated methodologies[12–17] have made it possible to calculate typical reaction pathways, such as intrinsic reaction coordinates (IRCs).[18] Thus, the basic tools necessary for MO-based reaction mechanism analysis are already available. However, it must be remembered that the definition of MO is not unique, and due to its arbitrariness, it is necessary to select an appropriate definition for the purpose of analysis. This arbitrariness of MO comes from the invariance of the wavefunction to orbital rotations. For example,

the Hartree–Fock wavefunction is invariant to transformations that rotate occupied and virtual orbitals separately.[19] This situation could be compared to a choice of coordinate axes. It is very common to choose a coordinate axis that is convenient for describing the system to be analyzed, e.g., applying classical multidimensional scaling methods[20,21] or principal component analysis[22] to chemical reaction analysis. Such a choice of characteristic coordinate axes is allowed because the rotation of the coordinate axes never changes the nature of the data. Rotation of the coordinate axes only changes the way the data are represented and labeled. Thus, choosing the appropriate coordinate axes often highlights the essence of the data without changing the nature of the system. Given this invariance, it is no more beneficial to insist on a particular definition of MO than it is to insist on a particular coordinate. It is also pointed out that there does not exist an optimal definition of MO for any given analysis.[23] For example, even the well-known frontier orbitals of the canonical molecular orbital (CMO), the diagonal basis of the Fock matrix, do not correlate well with the polarizability, contrary to conventional understanding.[11] Since the analysis of MOs is meaningful as long as the MOs appropriately characterize the subject of analysis, it is essential to choose an appropriate definition of MOs for the purpose of analysis.

In order to understand and characterize the various chemical properties of many-body wavefunctions, a great number of orbital definitions have been introduced: natural orbital (NO),[24] localized orbital (LO),[25] interacting frontier orbitals (IFOs),[26] natural bond orbital (NBO),[27] natural localized molecular orbitals (NLMOs),[28] intrinsic bond orbitals (IBOs),[29] valence virtual orbitals (VVOs),[30] principal interacting orbitals (PIOs),[31] and energy natural orbitals (ENOs).[32] All of these methods are useful for characterizing the static nature of many-body wavefunctions at a single geometrical structure, but by definition, there are no molecular orbitals that directly characterize changes in electron density along a reaction pathway. Considering that pushing-arrow diagram, a common technique for describing reaction mechanisms in organic chemistry, schematically show the electron flow in (elementary) chemical reactions, it seems quite natural to design MOs for reaction mechanism analysis and characterize electron density changes along reaction coordinates. However, if MOs that are not suitable for the analysis of electron density changes are used, the contribution to electron density changes may be distributed among many MOs, making orbital-based reaction mechanism analysis difficult.

Recently, we proposed a new type of molecular orbital designed for chemical reaction analysis, the natural reaction orbital (NRO).[33] Actually, we recently noted that the terminology, natural reaction orbital (NRO), was first used by Ruedenberg *et al.*[34,35] as the natural orbital basis within full reaction space. In order to avoid confusion, it should be declared that our "NRO" is a concept different from their "NRO." The NRO is obtained by applying singular value decomposition (SVD), first applied to orbital transformations by Amos and Hall,[36] to the first-order orbital response to nuclear coordinate perturbations given by the coupled-perturbed self-consistent filed (CPSCF) equation.[37–39] The orbitals obtained by applying SVD to the CPSCF with respect to charge fluctuations are known as intrinsic soft molecular orbitals (ISMOs).[40] ISMO is the optimal basis for characterizing electron density changes due to partial charge fluctuations. Similarly, NRO can be considered as the optimal basis for characterizing electron density changes due to changes in molecular geometry. Indeed, NRO could successfully characterize various types of chemical reactions without having to track orbitals along the reaction pathway. Moreover, NRO can automatically extract representative orbitals of a given chemical reaction based on the magnitude of the singular values of occupied-virtual NRO pairs, which measure the mixing rate of the NRO pairs. Interestingly, the product of NRO pairs can indicate the electron density change due to the mixing of the pairs. Thus, NRO can not only identify representative orbitals, but it also describes the changes induced by representative orbitals without manual work based on in-depth knowledge of chemistry. This is the main reason why NRO is suitable for reaction analysis.

Although NRO was successfully applied to typical reactions in the ground state, the applicability of the NRO method was limited to electronic structure theory based on a single-determinant configuration. Accordingly, chemical reactions involving explicit bond dissociation and formation processes that require multiconfigurational wavefunctions could not be analyzed by NRO. Thus, there is a need for another practical method of orbital analysis that can be applied to multiconfigurational theory[41,42] and linear response theory as well.[43–45]

In this study, we extend the NRO to a multiconfigurational theory, called multiconfiguration NRO (MC-NRO); MC-NRO is not equivalent to NRO, but it is possible to automatically extract representative orbitals of a given reaction even in electronically excited states at a moderate computational cost.

Section II describes the formulation of the MC-NRO method. Section III then presents five application examples and discussion. In the respective examples, it is shown that the MC-NRO method successfully characterizes the reaction. A discussion of the symmetry of the MC-NRO is also included in Sec. III and the supplementary material.

## II. MULTICONFIGURATION NATURAL REACTION ORBITAL

### A. Natural reaction orbital for Hartree–Fock theory

First, a brief description of the NRO formulation for the Hartree–Fock (HF) method is given. The detailed formulation is given in our previous report.[33] Let $\Phi$ denote the HF wavefunction for a given geometry and the first-order response of the HF wavefunction to nuclear coordinate displacements, $\Phi^{(1)}$, be given by[39]

$$\left|\Phi^{(1)}\right\rangle = \sum_{\substack{a\in \mathrm{vir}\\ i\in \mathrm{occ}}} U_{ai}^{(1)} a_a^\dagger a_i |\Phi\rangle - \frac{1}{2}\sum_{i\in \mathrm{occ}} S_{ii}^{(1)} |\Phi\rangle, \tag{1}$$

where the matrix $U_{ai}^{(1)}$ is defined by

$$U_{ai}^{(1)} := \sum_{\mu\nu} c_{\mu a} S_{\mu\nu} c_{\nu i}^{(1)}. \tag{2}$$

The subscripts $\mu$ and $\nu$ are used for the atomic orbital (AO) basis. $S_{\mu\nu}$ is the overlap matrix, $c_{\mu a}$ is the $a$-th virtual canonical orbital coefficient, and $c_{\nu i}^{(1)}$ is the first-order response to the nuclear coordinate displacement of the $i$-th occupied canonical orbital. The operators $a_i$ and $a_a^\dagger$ in Eq. (1) are the annihilation and creation operators for

$i$-th occupied and $a$-th virtual canonical orbitals, respectively. $S_{ii}^{(1)}$ in Eq. (1) is defined as

$$S_{ii}^{(1)} := \sum_{\mu\nu} c_{\mu i} S_{\mu\nu}^{(1)} c_{\nu i}, \tag{3}$$

where $S_{\mu\nu}^{(1)}$ is the first-order response of the overlap matrix. The second term in Eq. (1) comes from the orthonormalization condition of the occupied orbitals and is not considered essential for understanding chemical reactivity. Then, we will use only the virtual-occupied block of the first-order response given by

$$\left\langle \Phi^{(1)} \middle| a_a^\dagger a_i \middle| \Phi \right\rangle = U_{ai}^{(1)} \tag{4}$$

to characterize the response of the HF wavefunction to the nuclear coordinate displacement. The first-order response matrix $U_{ai}^{(1)}$ is obtained by solving the CPSCF equations.

A suitable molecular orbital basis for characterizing the first-order response matrix in Eq. (4) is given by SVD. For a given $U_{ai}^{(1)}$, a couple of unitary transformations can be found,

$$\mathbf{U}_{\mathrm{VO}}^{(1)} = \mathbf{L}\mathbf{\Lambda}\mathbf{R}^\dagger, \tag{5}$$

where $\mathbf{U}_{\mathrm{VO}}^{(1)}$ is defined by

$$\mathbf{U}_{\mathrm{VO}}^{(1)} := \sum_{\substack{a\in \mathrm{vir} \\ i\in \mathrm{occ}}} U_{ai}^{(1)} \boldsymbol{c}_a \otimes \boldsymbol{c}_i. \tag{6}$$

$\mathbf{L}$ and $\mathbf{R}$ are unitary matrices of size $N_{\mathrm{vir}} \times N_{\mathrm{vir}}$ and $N_{\mathrm{occ}} \times N_{\mathrm{occ}}$, respectively. $N_{\mathrm{occ}}$ and $N_{\mathrm{vir}}$ are the number of occupied and virtual orbitals, respectively. $\mathbf{\Lambda}$ is a rectangular matrix of size $N_{\mathrm{vir}} \times N_{\mathrm{occ}}$ with nonnegative singular values $\left(\lambda_1, \ldots, \lambda_{\min(N_{\mathrm{occ}}, N_{\mathrm{vir}})}\right)$ in the diagonal elements. In the SVD process, occupied and virtual orbitals are transformed separately,

$$\begin{cases} (\boldsymbol{n}_1, \ldots, \boldsymbol{n}_{N_{\mathrm{occ}}}) = (\boldsymbol{c}_1, \ldots, \boldsymbol{c}_{N_{\mathrm{occ}}})R, \\ (\boldsymbol{n}'_1, \ldots, \boldsymbol{n}'_{N_{\mathrm{vir}}}) = (\boldsymbol{c}_{N_{\mathrm{occ}}+1}, \ldots, \boldsymbol{c}_{N_{\mathrm{occ}}+N_{\mathrm{vir}}})L. \end{cases} \tag{7}$$

Using the generated occupied and virtual basis, $(\boldsymbol{n}_1, \ldots, \boldsymbol{n}_{N_{\mathrm{occ}}})$ and $\left(\boldsymbol{n}'_1, \ldots, \boldsymbol{n}'_{N_{\mathrm{vir}}}\right)$, $\mathbf{U}_{\mathrm{VO}}^{(1)}$ can be written as

$$\mathbf{U}_{\mathrm{VO}}^{(1)} = \sum_{i=1}^{\min(N_{\mathrm{occ}}, N_{\mathrm{vir}})} \lambda_i \boldsymbol{n}'_i \otimes \boldsymbol{n}_i. \tag{8}$$

Here, it will be clear that the occupied and virtual basis sets with the same subscripts form a pair and share a common singular value $\lambda_i$. There is no coupling term between the basis sets with different subscripts. Thus, the SVD basis of $\mathbf{U}_{\mathrm{VO}}^{(1)}$ can simplify the relationship between virtual and occupied orbitals for a given nuclear coordinate displacement. In other words, the SVD basis is the best basis for simplifying response density matrices. The NRO is the SVD basis pair given by Eq. (7) with nonzero singular values.

## B. Straightforward generalization of natural reaction orbital to multiconfigurational theory

The generalization of NRO to multiconfigurational theory is simple in the formula. Let $\Psi$ be an arbitrary multiconfigurational wavefunction. The first-order response density matrix for nuclear coordinate displacements given by

$$\left\langle \Psi^{(1)} \middle| a_p^\dagger a_q \middle| \Psi \right\rangle \tag{9}$$

is used to characterize the change in the wavefunction. Here, the subscripts $p$ and $q$ are used for all molecular orbital basis. Evaluating the matrix in Eq. (9) requires derivatives of the configuration interaction coefficients with respect to the nuclear coordinates. The computational cost for this term would be quite large, and it is not easy to adopt Eq. (9) as is. Therefore, it is necessary to introduce a more practical formulation that is different from the straightforward generalization.

## C. Definition for CASSCF

In this subsection, we will define the molecular orbitals that characterize the electronic density change along a given reaction coordinate in the framework of the complete active space self-consistent field (CASSCF) theory. First, it is necessary to clarify how the electron density change will be represented in this study. The AO density matrix $\mathbf{D}_{\mathrm{AO}}$ is positive semi-definite. Thus, there exists one positive semi-definite square root of $\mathbf{D}_{\mathrm{AO}}$,[46,47] denoted as $\mathbf{D}_{\mathrm{AO}}^{1/2}$, which satisfies the following condition:

$$\mathbf{D}_{\mathrm{AO}} = \mathbf{D}_{\mathrm{AO}}^{1/2} \mathbf{D}_{\mathrm{AO}}^{1/2}. \tag{10}$$

In general, the trace of the AO density matrix does not give the total number of electrons, $n_{\mathrm{total}}$, which is given by

$$n_{\mathrm{total}} = \mathrm{tr}(\mathbf{D}_{\mathrm{AO}}\mathbf{S}), \tag{11}$$

where $\mathbf{S}$ is the overlap matrix. Since the overlap matrix is also positive semi-definite, we can define its square root, $\mathbf{S}^{1/2}$. Then, the trace of the Hermitian matrix gives the total number of electrons,

$$\tilde{\mathbf{D}} := \mathbf{S}^{1/2}\mathbf{D}_{\mathrm{AO}}\mathbf{S}^{1/2} = \mathbf{S}^{1/2}\mathbf{D}_{\mathrm{AO}}^{1/2}\mathbf{D}_{\mathrm{AO}}^{1/2}\mathbf{S}^{1/2}. \tag{12}$$

Since the total number of electrons does not change with geometrical structure change, the trace of the matrix $\tilde{\mathbf{D}}$ is constant,

$$\frac{d}{d\tau}\mathrm{tr}\left(\tilde{\mathbf{D}}\right) = 0, \tag{13}$$

where $\tau$ is an arbitrary reaction coordinate. Equation (13) implies that conservation of the total number of electrons holds for a given nuclear coordinate change. The derivative of $\tilde{\mathbf{D}}$ along the reaction coordinate is given by

$$\frac{d}{d\tau}\tilde{\mathbf{D}} = \frac{d}{d\tau}\left(\mathbf{S}^{1/2}\mathbf{D}_{\mathrm{AO}}^{1/2}\right)\mathbf{D}_{\mathrm{AO}}^{1/2}\mathbf{S}^{1/2} + (\mathrm{h.c.}), \tag{14}$$

where (h.c.) stands for Hermite Conjugate. Apparently, the derivative of $\tilde{\mathbf{D}}$ includes the derivative of $\mathbf{S}^{1/2}$. Essentially, the derivative of the overlap matrix should not be interpreted as MO mixing but simply as AO translation. Then, the derivative of $\mathbf{S}^{1/2}$ would seem unnecessary for evaluating MO mixing. However, the derivative of $\mathbf{S}^{1/2}$ is necessary to satisfy Eq. (13). To solve this problem, the derivative terms of $\mathbf{S}^{1/2}$, $\left(\frac{d}{d\tau}\mathbf{S}^{1/2}\right)\mathbf{D}_{\mathrm{AO}}\mathbf{S}^{1/2}$, are approximated as

$$\begin{aligned}\mathbf{Y}_{\mathrm{CASSCF}} := &\frac{1}{N_{\mathrm{inactive}}} tr\left(\mathbf{C}_{\mathrm{inactive}}^{\dagger}\mathbf{S}^{1/2}\left(\frac{d}{d\tau}\mathbf{S}^{1/2}\right)\mathbf{D}_{\mathrm{AO}}\mathbf{S}\mathbf{C}_{\mathrm{inactive}}\right)\mathbf{I}_{\mathrm{inactive}}\\ &+\frac{1}{N_{\mathrm{inactive}}} tr\left(\mathbf{C}_{\mathrm{inactive}}^{\dagger}\mathbf{S}^{1/2}\left(\frac{d}{d\tau}\mathbf{S}^{1/2}\right)\mathbf{D}_{\mathrm{AO}}\mathbf{S}\mathbf{C}_{\mathrm{inactive}}\right)\mathbf{I}_{\mathrm{inactive}}\\ &+\frac{1}{N_{\mathrm{secondary}}} tr\left(\mathbf{C}_{\mathrm{secondary}}^{\dagger}\mathbf{S}^{1/2}\left(\frac{d}{d\tau}\mathbf{S}^{1/2}\right)\mathbf{D}_{\mathrm{AO}}\mathbf{S}\mathbf{C}_{\mathrm{secondary}}\right)\mathbf{I}_{\mathrm{secondary}},\end{aligned} \tag{15}$$

where $\mathbf{C}_{\mathrm{inactive}}$, $\mathbf{C}_{\mathrm{active}}$, and $\mathbf{C}_{\mathrm{secondary}}$ are the MO coefficients and $\mathbf{I}_{\mathrm{inactive}}$, $\mathbf{I}_{\mathrm{active}}$, and $\mathbf{I}_{\mathrm{secondary}}$ are the identity matrices for inactive (doubly occupied), active, and secondary (unoccupied) spaces.[42] $N_{\mathrm{inactive}}$, $N_{\mathrm{active}}$, and $N_{\mathrm{secondary}}$ are the number of MOs in each space. Finally, we evaluate the density change due to nuclear coordinate displacement as

$$\mathbf{X}_{\mathrm{CASSCF}} := \mathbf{C}^{\dagger}\mathbf{S}\left(\frac{d}{d\tau}\mathbf{D}_{\mathrm{AO}}^{1/2}\right)\mathbf{D}_{\mathrm{AO}}^{1/2}\mathbf{S}\mathbf{C} + \mathbf{Y}_{\mathrm{CASSCF}} \tag{16}$$

and its Hermitian conjugate ($\mathbf{C}$ is the entire MO coefficient matrix). A more compact description of the matrix in Eq. (16) can be found in the supplementary material. In fact, the derivative can be approximated by numerical differentiation, e.g., $d\mathbf{D}_{\mathrm{AO}}^{1/2}/d\tau \sim (2\Delta\tau)^{-1}\left\{\mathbf{D}_{\mathrm{AO}}^{1/2}(\Delta\tau) - \mathbf{D}_{\mathrm{AO}}^{1/2}(-\Delta\tau)\right\}$, where $\Delta\tau$ is the step size of the numerical differentiation. In this work, all derivatives in Eq. (16) are evaluated numerically.

The MC-NRO for CASSCF is defined as the SVD basis for the secondary-active, secondary-inactive, active–active, and active–inactive blocks of $\mathbf{X}_{\mathrm{CASSCF}}$. To separate $\mathbf{X}_{\mathrm{CASSCF}}$ into blocks, the MO used to define the active space, e.g., NO, may be useful. Each SVD basis characterizes the density change of each block. For example, the SVD basis of a secondary-active block characterizes the electron transfer from the active space to the secondary space. In particular, the SVD basis for the off-diagonal blocks of the secondary-active, secondary-inactive, and active–inactive blocks is interpreted as the optimal basis to characterize the orbital mixing between the two spaces. On the other hand, the SVD basis for the active–active block includes the contribution to the electron density change of the change in the CI coefficient as well as the change in the MO coefficient. Therefore, the contribution of the diagonal block cannot necessarily be interpreted as pure MO mixing. This point will be discussed in detail in Sec. III. The above definition can be applied to state-averaged (SA) CASSCF[48] as well as state-specific (SS) CASSCF. In the case of SA-CASSCF, the density matrix of each root can be used to calculate the MC-NRO. However, it is necessary to carefully check whether the orbitals optimized by the SA-CASSCF method provide a balanced description of the multi-state potential energy surfaces.[49]

The reason for separate SVD, or orbital rotation, for the four blocks of the $\mathbf{X}_{\mathrm{CASSCF}}$ matrix requires explanation. If the separation were not done, MOs defined in distinguished spaces, such as MOs in secondary space and MOs in active space, could be mixed due to unitary transformations in SVD process. However, the CASSCF wavefunction is not invariant to the mixing of MOs in distinguished spaces.[42,50] Thus, SVD without separation changes the wavefunction and destroys the physical nature of the system. From the viewpoint of analysis, the loss of nature of the system does not seem desirable. In other words, when performing SVD, the separation should be performed in such a way that the orbital invariance of the CASSCF wavefunction is not lost.

Next, we explain the density change expressed in the MC-NRO basis. The right and left MC-NROs are given by

$$\begin{cases}\left(\phi_1^{\mathrm{sR}},\ldots,\phi_{N_{\mathrm{s}}}^{\mathrm{sR}}\right) = \left(\psi_1^{\mathrm{s}},\ldots,\psi_{N_{\mathrm{s}}}^{\mathrm{s}}\right)\mathbf{R}^{\dagger},\\ \left(\phi_1^{\mathrm{tL}},\ldots,\phi_{N_{\mathrm{t}}}^{\mathrm{tL}}\right) = \left(\psi_1^{\mathrm{t}},\ldots,\psi_{N_{\mathrm{t}}}^{\mathrm{t}}\right)\mathbf{L},\end{cases} \tag{17}$$

where $\left(\psi_1^{\mathrm{s}},\ldots,\psi_{N_{\mathrm{s}}}^{\mathrm{s}}\right)$ and $\left(\psi_1^{\mathrm{t}},\ldots,\psi_{N_{\mathrm{t}}}^{\mathrm{t}}\right)$ are the MOs in subsets s (e.g., active space) and t (e.g., secondary space), respectively, and $N_{\mathrm{s}}$ and $N_{\mathrm{t}}$ are the number of MOs in the respective spaces. The matrices $\mathbf{R}$ and $\mathbf{L}$ are the right and left singular vectors of the t-s block of the matrix $\mathbf{X}$. The right and left singular vectors of $\mathbf{X}$ are included as rows and columns of $\mathbf{R}$ and $\mathbf{L}$. Then,

$$\lambda_i\left(\phi_i^{\mathrm{tL}*}\phi_i^{\mathrm{sR}} + \phi_i^{\mathrm{tL}}\phi_i^{\mathrm{sR}*}\right) = 2\lambda_i\phi_i^{\mathrm{tL}}\phi_i^{\mathrm{sR}}\ (i = 1,\ldots,\min(N_{\mathrm{s}},N_{\mathrm{t}})) \tag{18}$$

gives the component of the density change induced by the displacement of the nuclear coordinates. Here, the orbitals are assumed to be real. The contribution of the derivative of the overlap matrix to the density change is evaluated in its trace [see Eq. (15)]. The singular value of each MC-NRO pair represents the extent to which the pair contributes to the density change. As the nature of SVD, the sum of squares of singular values is equal to the square of Frobenius norm of the matrix to be decomposed, the sum of squares of all the matrix elements. The square of Frobenius norm of the given block of matrix $\mathbf{X}$ gives the sum of the squares of density change or orbital mixing rates within the block. Throughout this work, we use the square of Frobenius norm to evaluate the total density change or orbital mixing rates along reaction pathways. Usually, only a small number of MC-NRO pairs have large singular values, and the density changes can only be characterized by such pairs. The relative phase of all MC-NRO pairs is uniquely determined for a given nuclear displacement direction.[33] Reversing the displacement direction inverts the relative phase of all MC-NRO pairs.

It should be noted that the singular values are computed by numerically differentiating the density matrix and are, therefore, not very numerically stable. Although the shape of the dominant MC-NRO is not so unstable, singular values can be unstable in cases such as CASSCF. To extract the qualitative essence of a chemical reaction, the MC-NRO method using numerical differentiation is effective.

In general, the value $\Delta_i$ defined by the following equation can have a nonzero value if the subsets s and t are identical:

$$\Delta_i := \lambda_i\left(\left\langle\phi_i^{\mathrm{tL}}|\phi_i^{\mathrm{sR}}\right\rangle + \left\langle\phi_i^{\mathrm{sR}}|\phi_i^{\mathrm{tL}}\right\rangle\right), \tag{19}$$

where $\langle\phi_i^{\mathrm{tL}}|\phi_i^{\mathrm{sR}}\rangle$ is the inner product of $\phi_i^{\mathrm{tL}}$ and $\phi_i^{\mathrm{sR}}$. Conversely, $\Delta_i$ is always zero when the two subsets are different. Regardless

of whether the two subspaces are identical or not, the following equation holds:

$$\sum_i \Delta_i = 0. \tag{20}$$

Actually, $\Delta_i$ can be considered as the change of occupation number in $\phi_i^{\mathrm{sR}}$ due to the change of CI coefficients. This point will be discussed in detail in Sec. III.

## III. RESULTS AND DISCUSSION

Here, the MC-NRO analysis is applied to five reaction examples: covalent bond formation of $H_2$, triple bond formation of $N_2$, Diels–Alder reaction of ethylene and 1,3-butadiene, [1,5]-sigmatropic rearrangement of 1,3-pentadiene, and intramolecular hydrogen transfer of malonaldehyde in the $S_1$ state. We will demonstrate how the new approach can be used to understand chemical reaction processes in terms of electron transfer and discuss future challenges. All calculations were performed in Gaussian 16 Rev.C.01.[51]

### A. Hydrogen molecule

As a simple example, the MC-NRO analysis of the covalent bond formation of $H_2$ is demonstrated. The main purpose of this demonstration is to confirm that the MC-NRO method provides a reasonable picture that is consistent with conventional understanding provided by other methods, e.g., natural orbitals. The bond formation process of $H_2$ is so simple that it is considered the best system to validate the MC-NRO method and to understand how it works. It is well known that the dissociated state of H···H cannot be described by a single-determinant wavefunction, e.g., the Slater determinant given by the Hartree–Fock theory.[52,53] Thus, this process needs to be studied with a multiconfigurational wavefunction. The potential energy curve for the singlet ground state (black curve) of $H_2$ at CASSCF(2,2)/aug-cc-pVQZ[54,55] is shown in Fig. 1. The sum of squares of the singular values of MC-NRO, which indicate the degree of electron density change, is shown for two blocks: active–active and secondary-active blocks. The density change in active space is larger in two regions: A ($R \sim 2.10$ Å) and B ($R < 1.20$ Å), where $R$ is the bond length of the hydrogen molecule.

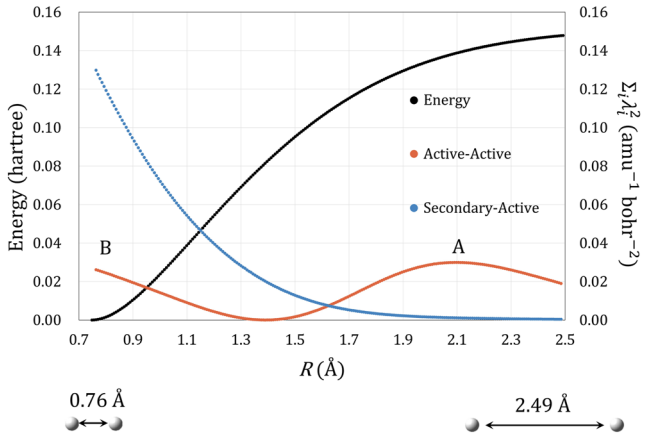


**FIG. 1.** Potential energy curve of the singlet ground state of the hydrogen molecule (black curve) and the sum of squares of the singular values of the MC-NROs for the two blocks of active–active (red curve) and secondary-active (blue curve) (shown as $\sum_i \lambda_i^2$). The electronic structure is computed at the CASSCF(2,2)/aug-cc-pVQZ level. A and B are the characteristic regions where the sum of squares of the singular values shows an outstandingly large value.

The dominant MC-NRO pairs and the corresponding density changes in the two regions are shown in Fig. 2. The direction of nuclear displacements is in the direction of bond formation. The dominant MC-NRO pairs in region A are the antibonding orbital ($\sigma_u^*$) pair with the opposite sign and the bonding orbital ($\sigma_g$) pair with the same sign. Since the product of the right and left MC-NROs gives an electron density change in the direction of molecular formation, the electron density of the antibonding $\sigma_u^*$ orbital pair decreases and that of the bonding $\sigma_g$ orbital pair increases as the bond length $R$ decreases. These density changes clearly correspond to the formation of H–H covalent bond.

The opposite-phase interference of the $\sigma_u^*$ orbital and in-phase interference of the $\sigma_g$ orbital are interpreted as follows: In the dissociation limit, the two electron wavefunction of $H_2$ for the singlet ground state is given by a linear combination of two Slater determinants as follows:[56]

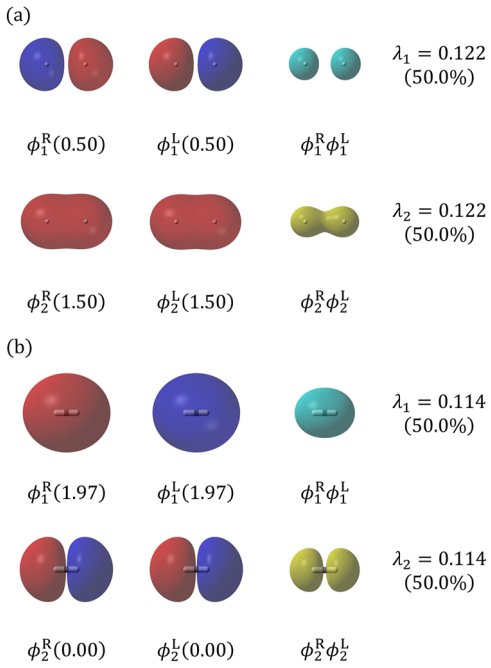


**FIG. 2.** Active–active MC-NRO pairs for H–H covalent bond formation at (a) $R = 2.10$ Å and (b) $R = 0.77$ Å. $\phi_i^{\mathrm{R}}$ and $\phi_i^{\mathrm{L}}$ denote the $i$th right and left MC-NROs, and the numbers in parentheses indicate the occupation number. The product of each MC-NRO pair is also shown, with the yellow/cyan colors indicating increasing/decreasing electron density. $\lambda_i$ $\left(\mathrm{amu}^{-1/2}\,\mathrm{bohr}^{-1}\right)$ indicates the singular value of the $i$th MC-NRO pair. The contribution of the MC-NRO pair to the density change of active–active block, defined as $100 \times \lambda_i^2 / \sum_j \lambda_j^2$, is also shown for each singular value. The isovalues of MC-NRO and density change are 0.0250 and 0.006 25, respectively.

$$\Psi_{R\to\infty}(1,2) = \frac{1}{2}\begin{vmatrix} \chi^{1s}_{H_A}(1)\alpha(1) & \chi^{1s}_{H_B}(1)\beta(1) \\ \chi^{1s}_{H_A}(2)\alpha(2) & \chi^{1s}_{H_B}(2)\beta(2) \end{vmatrix} + \frac{1}{2}\begin{vmatrix} \chi^{1s}_{H_B}(1)\alpha(1) & \chi^{1s}_{H_A}(1)\beta(1) \\ \chi^{1s}_{H_B}(2)\alpha(2) & \chi^{1s}_{H_A}(2)\beta(2) \end{vmatrix} = \frac{1}{2}\{\chi^{1s}_{H_A}(1)\chi^{1s}_{H_B}(2) + \chi^{1s}_{H_B}(1)\chi^{1s}_{H_A}(2)\} \times \{\alpha(1)\beta(2) - \beta(1)\alpha(2)\}, \quad (21)$$

where $\chi^{1s}_{H_A}$ and $\chi^{1s}_{H_B}$ are the normalized 1s orbitals of the two hydrogen atoms $H_A$ and $H_B$, and $\alpha$ and $\beta$ are spin functions. By rotating the orbitals,

$$\begin{bmatrix} \sigma_g \\ \sigma_u^* \end{bmatrix} = \frac{1}{\sqrt{2}}\begin{bmatrix} 1 & 1 \\ -1 & 1 \end{bmatrix}\begin{bmatrix} \chi^{1s}_{H_A} \\ \chi^{1s}_{H_B} \end{bmatrix}, \quad (22)$$

the wavefunction is rewritten as

$$\Psi_{R\to\infty}(1,2) = \frac{1}{2}\begin{vmatrix} \sigma_g(1)\alpha(1) & \sigma_g(1)\beta(1) \\ \sigma_g(2)\alpha(2) & \sigma_g(2)\beta(2) \end{vmatrix} - \frac{1}{2}\begin{vmatrix} \sigma_u^*(1)\alpha(1) & \sigma_u^*(1)\beta(1) \\ \sigma_u^*(2)\alpha(2) & \sigma_u^*(2)\beta(2) \end{vmatrix}. \quad (23)$$

Around the equilibrium bond length, the HF wavefunction given by a single Slater determinant is known to give a good approximation,

$$\Psi_{R_{eq}}(1,2) \sim \frac{1}{\sqrt{2}}\begin{vmatrix} \sigma_g(1)\alpha(1) & \sigma_g(1)\beta(1) \\ \sigma_g(2)\alpha(2) & \sigma_g(2)\beta(2) \end{vmatrix}. \quad (24)$$

Using the CI coefficients, $C_1$ and $C_2$, the wavefunction with the minimal basis can be rewritten as

$$\Psi(1,2) = C_1\begin{vmatrix} \sigma_g(1)\alpha(1) & \sigma_g(1)\beta(1) \\ \sigma_g(2)\alpha(2) & \sigma_g(2)\beta(2) \end{vmatrix} + C_2\begin{vmatrix} \sigma_u^*(1)\alpha(1) & \sigma_u^*(1)\beta(1) \\ \sigma_u^*(2)\alpha(2) & \sigma_u^*(2)\beta(2) \end{vmatrix}. \quad (25)$$

Then, $|C_1|^2$ increases toward the equilibrium structure while $|C_2|^2$ decreases. In the bond formation process where the symmetry of the system is preserved, $\sigma_g$ and $\sigma_u^*$ belong to different irreducible representations and do not mix with each other. Therefore, the electron density change in this process is not due to orbital mixing but to a change in the CI coefficient. Nevertheless, the density change can be described by the MO norm change. That is, the change in the weight of the configuration can be described by an increase or decrease in the norm of $\sigma_g/\sigma_u^*$, rather than an increase or decrease in $|C_1|^2/|C_2|^2$. Thus, the opposite-phase interference of the $\sigma_u^*$ orbital and the in-phase interference of the $\sigma_g$ orbital correspond to a decrease in the weight of the doubly excited-state configuration and an increase in the ground-state configuration, respectively. This result indicates that MC-NRO provides a way to express the change in electron density due to CI coefficient change in terms of MO. The dominant MC-NRO pair in region B shows an opposite density change, a decrease/increase in $\sigma_g/\sigma_u^*$, possibly working to mitigate the repulsion between electrons. However, this behavior may be an artifact due to the small active space. This will be discussed in more detail later.

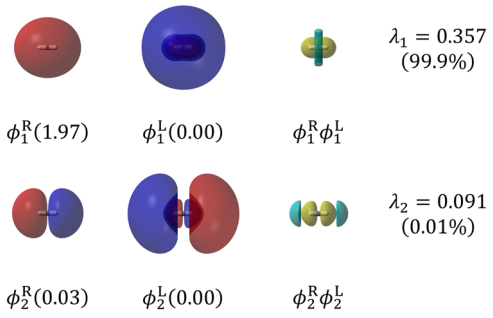


**FIG. 3.** Secondary-active MC-NRO pairs with H–H covalent bond formation at $R = 0.77$ Å. $\phi_i^R$ and $\phi_i^L$ represent the $i$th right and left MC-NRO, and the numbers in parentheses indicate the occupation number. The product of each MC-NRO pair is also shown, with the yellow/cyan color indicating increasing/decreasing electron density. $\lambda_i\left(\text{amu}^{-1/2}\,\text{bohr}^{-1}\right)$ represents the singular value of the $i$th MC-NRO pair. Also shown below each singular value is the contribution of the MC-NRO pair to the overall density change. The isovalues of MC-NRO and density change are 0.0250 and 0.006 25, respectively.

The dominant secondary-active MC-NRO pair in the region B, $\phi_1^R$ and $\phi_1^L$, is composed of bonding $\sigma_g$ orbitals, one composed of 1s orbitals and the other of 2s orbitals (Fig. 3). These two $\sigma_g$ orbitals are in-phase near the H–H bond axis, but they are out-of-phase in the outer region. The product of the MC-NRO pair gives a density change, which means that the MC-NRO pair condenses the electron density around the H–H bond axis and reduces the nuclear repulsion.

In region B, there is a remarkable density change due to missing of the secondary-active MC-NRO, indicating that the active

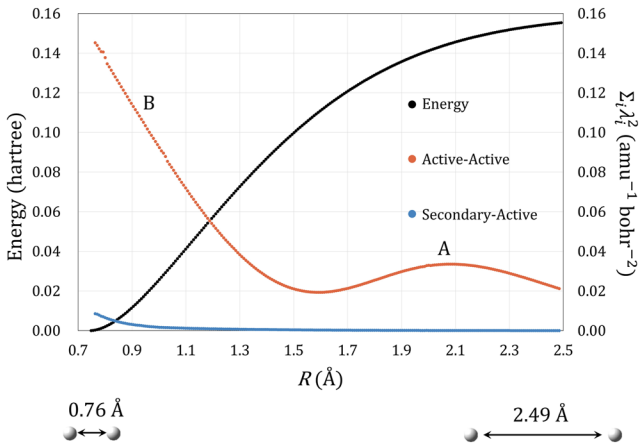


**FIG. 4.** Potential energy curve of the singlet ground state of hydrogen molecule (black curve) and the sum of squares of the singular values of MC-NROs for the two blocks of active–active (red curve) and secondary-active (blue curve) (denoted by $\sum_i\lambda_i^2$) as a function of H···H distance. The electronic structure is calculated at the CASSCF(2,10)/aug-cc-pVQZ level. A and B are the characteristic regions where the sum of squares of the singular values shows outstandingly large value.

space is not closed in the H–H bond formation process. Ideally, the active space of CASSCF should be set large enough to describe any dominant change during the chemical reaction. From this viewpoint, a large orbital mixing between the active space and inactive or secondary spaces is undesirable. In this study, preliminary CASSCF calculations were performed to check the convergence of the CASSCF calculations, and converged results were obtained with CASSCF(2,10)/aug-cc-pVQZ. The orbitals of this active space are shown in the supplementary material. Figure 4 shows the result with CASSCF(2,10)/aug-cc-pVQZ. Compared to Fig. 1, it can be seen that the mixing of the active and secondary space orbitals is significantly reduced.

Figure 5 shows the dominant MC-NRO pairs. In region A, the dominant MC-NRO pair is almost the same as in Fig. 2(a), while in region B, the dominant MC-NRO pairs are different from those shown in Fig. 2(b) but rather similar to the first MC-NRO pair in Fig. 3. This indicates that the first left MC-NRO $\phi_1^{\mathrm{L}}$ shown in Fig. 3 is included in the expanded active space. Thus, the expanded active space can be considered to be more closed throughout the reaction process. Indeed, Fig. 6 suggests an improvement in the active space from the energy viewpoint as well. Figure 6 shows that the energy difference between the CASSCF(2,2) and CASSCF(2,10) results increases in the direction of bond formation. This feature may be explained in terms of radial correlations. The significance of radial correlations for the electron affinity of carbon, oxygen, and fluorine was reported by Botch and Dunnig.[57] Subsequently, Walch *et al.* studied the effect of radial correlation on the height of the reaction barrier in the reaction X + $H_2$ → XH + H (X = O, F).[58,59] In Ref. 58, an orbital basis with additional radial nodes was found to be important in describing the tight–diffuse correlation of anion-like oxygen atom around the transition state (TS) region. In the present

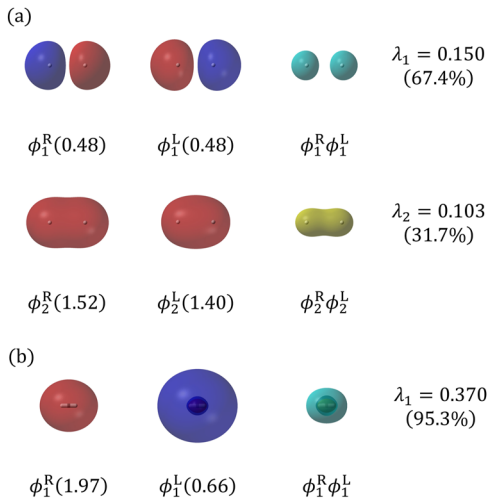


**FIG. 5.** The active–active MC-NRO pairs in the H–H covalent bond formation process: (a) $R$ = 2.08 Å; (b) $R$ = 0.77 Å. $\phi_i^{\mathrm{R}}$ and $\phi_i^{\mathrm{L}}$ represent the $i$th right and left MC-NROs and the numbers in parentheses indicate the occupation number. The product of each MC-NRO pair is also shown, with the yellow/cyan color representing the increase/decrease in electron density. $\lambda_i\left(\mathrm{amu}^{-1/2}\,\mathrm{bohr}^{-1}\right)$ denotes the singular value of the $i$th MC-NRO pair. Also shown below each singular value is the contribution of the MC-NRO pair to the overall density change. The isovalues of MC-NRO and density change are 0.0250 and 0.006 25, respectively.

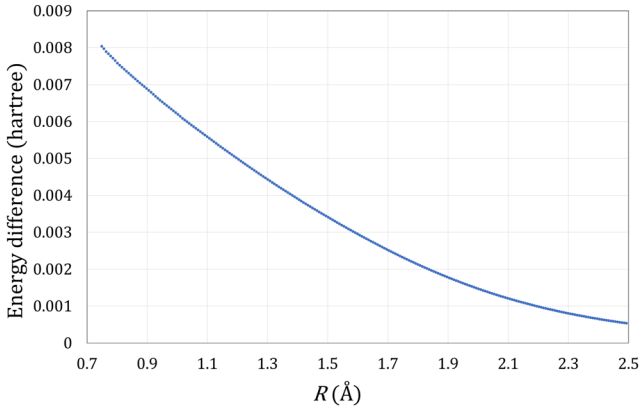


**FIG. 6.** Energy difference between CASSCF(2,2) and CASSCF(2,10) results.

homonuclear reaction H + H → $H_2$, the reactants, two hydrogen atoms with an isolated electron each, do not have radial tight–diffuse correlations, but the product, hydrogen molecule, does, and the radial tight–diffuse correlations increase. In fact, in the MC-NRO on the left in Fig. 5(b), there are extra radial nodes with nonzero occupancy, indicating the presence of tight–diffuse correlations.

Through the analysis of hydrogen molecule formation with different active spaces, it was shown that MC-NRO basis properly characterizes the density change along the covalent bond formation. Also, it should be reemphasized that the sum of squares of the singular values of MC-NRO can provide a kind of criterion to verify the quality of the active space in terms of electron density changes along the reaction path. Actually, the expanded active space was improved in terms of both density change and energy. Since the sum of square of singular values of MC-NROs is equal to square of the Frobenius norm of the matrices decomposed by SVD, validation of active space

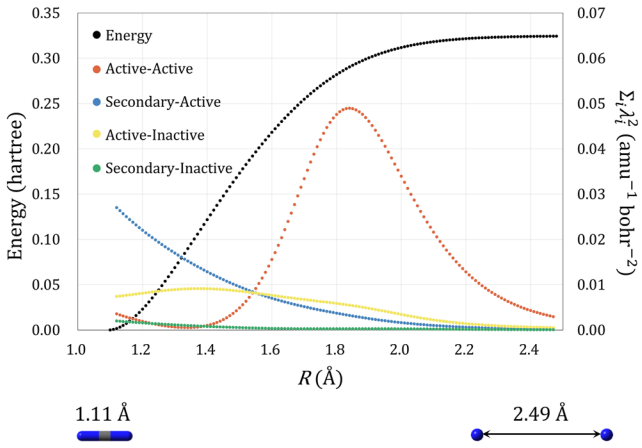


**FIG. 7.** Potential energy curve of the singlet ground state of the nitrogen molecule (black curve) and the sum of squares of the singular values of MC-NROs (denoted by $\sum_i \lambda_i^2$) for the four blocks, active–active (red curve), secondary-active (blue curve), active–inactive (yellow curve), and secondary-inactive (green) blocks, as a function of N···N distance. The electronic structure is calculated at the CASSCF(6,6)/cc-pVTZ level.

itself does not necessarily require the computation of MC-NROs. Thus, it will be sufficient for chemical reaction analysis to perform MC-NRO analysis only for the validated active space.

### B. Nitrogen molecule

As a second example, MC-NRO analysis was applied to the triple bond formation of $N_2$. The potential energy curve for the singlet ground state (black curve) of $N_2$ at CASSCF(6,6)/cc-pVTZ[54] is shown in Fig. 7. The active space consists of six 2p orbitals of two nitrogen atoms. The sum of squares of the singular values, indicating the degree of electronic density change, is also shown for the four blocks: active–active, secondary-active, active–inactive, and secondary-inactive blocks. While the active–active contribution is dominant at the early stages of bond formation, the secondary-active and active–inactive contributions are non-negligible near the equilibrium bond length. Thus, the active space consisting only of 2p orbitals seems to be unsatisfactory near equilibrium. However, it would be meaningful to investigate the cause of such poor behavior. Therefore, we first show an active–active MC-NRO that undergoes a bond formation process. Next, we show the secondary-active and active–inactive MC-NROs near equilibrium. Figure 8 shows the active–active MC-NROs for $R$ = 2.000 Å, which clearly shows the formation of a $\sigma$ bond, $\phi_1^{\mathrm{R}}\phi_1^{\mathrm{L}}$, and two $\pi$ bonds, $\phi_{4,5}^{\mathrm{R}}\phi_{4,5}^{\mathrm{L}}$.

Figure 9 shows the secondary-active and active–inactive MC-NROs at $R$ = 1.120 Å. The secondary MC-NROs with large singular values work to concentrate the electron density around the bonding region, as in the case of hydrogen molecule. This result indicates that AOs with higher principal quantum number than valence AOs work to concentrate the electron density around the nucleus and relax

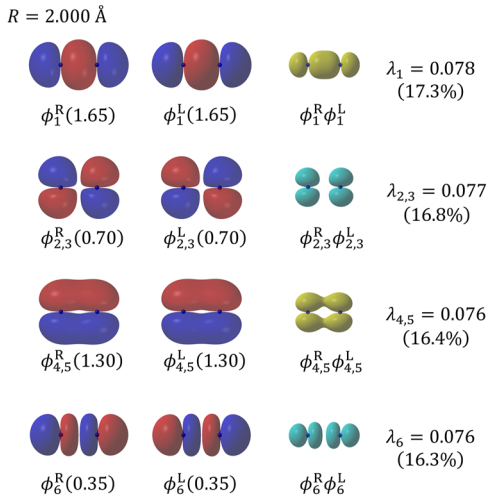


**FIG. 8.** The active–active MC-NRO pairs for the N–N triple bond formation for $R$ = 2.000 Å. $\phi_i^{\mathrm{R}}$ and $\phi_i^{\mathrm{L}}$ represent the $i$th right and left MC-NROs, and the numbers in parentheses indicate the occupation numbers. The product of each MC-NRO pair is also shown, with the yellow/cyan color representing the increase/decrease in electron density. $\lambda_i\left(\mathrm{amu}^{-1/2}\,\mathrm{bohr}^{-1}\right)$ denotes the singular value of the $i$th MC-NRO pair. Also shown below each singular value is the contribution of the MC-NRO pair to the overall density change. The isovalues of MC-NRO and density change are 0.020 and 0.004, respectively.

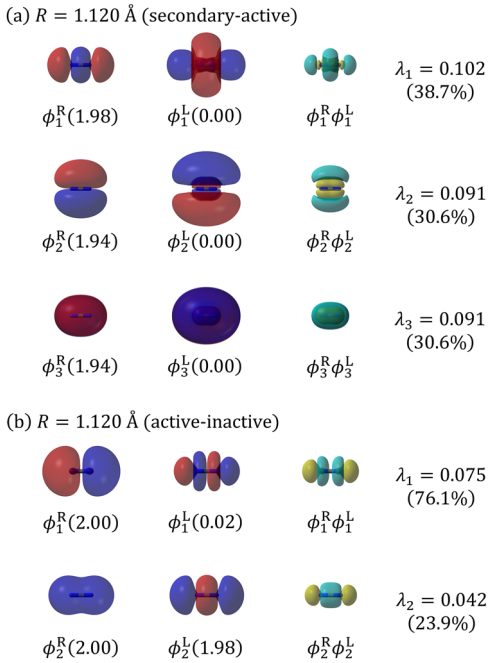


**FIG. 9.** (a) The dominant secondary-active and (b) active–inactive MC-NRO pairs for N–N triple bond formation at $R$ = 1.120 Å. $\phi_i^{\mathrm{R}}$ and $\phi_i^{\mathrm{L}}$ represent the $i$th right and left MC-NROs, and the numbers in parentheses indicate the occupation number. The product of each MC-NRO pair is also shown, with the yellow/cyan color representing the increase/decrease in electron density. $\lambda_i\left(\mathrm{amu}^{-1/2}\,\mathrm{bohr}^{-1}\right)$ denotes the singular value of the $i$th MC-NRO pair. Also shown below each singular value is the contribution of the MC-NRO pair to the overall density change. The isovalues of MC-NRO and density change are 0.020 and 0.004, respectively.

nuclear repulsion through the formation of covalent bonds. Therefore, it is ideal that AOs with one higher principal quantum number than the valence AOs relevant for bond formation should also be included in the active space. Inactive MC-NROs with large singular values are the $\sigma_{\mathrm{u}}{}^*$ and $\sigma_{\mathrm{g}}$ orbitals, which consist of 2s orbitals. The importance of these two orbitals may be understood in terms of sp hybridization. In summary, the active–inactive contribution is attributed to the use of a non-full-valence active space without 2s AOs, and the secondary-active contribution is attributed to the lack of an AO with one higher principal quantum number than the valence AO, which is important for density concentration around nuclei. Thus, the MC-NRO method can indicate which MOs should be added to the active space based on density changes along the reaction path. Although it is not easy to add all dominant MC-NROs to the active space due to computational costs, the MC-NRO method provides suggestions for improving the quality of the active space.

### C. Diels–Alder reaction

As a more practical example, the Diels–Alder reaction, which can be reproduced by a single-determinant wavefunction, was analyzed by the MC-NRO method. The purpose of this application is to confirm that the MC-NRO analysis is consistent with the conventional understanding of a well-studied reaction. The energy variation along the intrinsic reaction coordinate (IRC) for the Diels–Alder reaction of ethylene and 1,3-butadiene in the singlet ground state

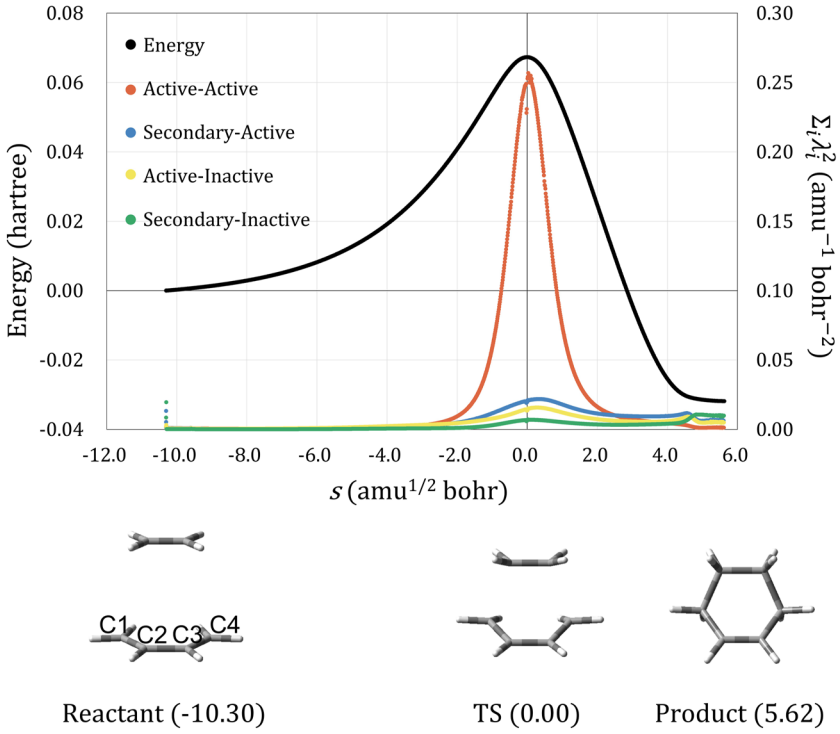


**FIG. 10.** Change of potential energy along the IRC of the Diels–Alder reaction of ethylene with 1,3-butadiene (black curve), as well as change of the sum of squares of singular values of MC-NRO for the active–active (red curve), secondary-active (blue curve), active–inactive (yellow curve), and secondary-inactive (green) blocks ($\sum_i \lambda_i^2$), at the CASSCF(8,7)/cc-pVTZ level. $s$ is the reaction coordinate. The geometries of reactants, TS, and products are shown with the values of the reaction coordinates.

(black curve) calculated at the CASSCF(8,7)/cc-pVTZ level is shown in Fig. 10. The $C_s$ symmetry is preserved along the IRC in this system. The sum of squares of the singular values, which indicate the degree of electron density change, is also shown for the four blocks: active–active, secondary-active, active–inactive, and secondary-inactive blocks. It can be seen that the active–active contribution is dominant throughout the IRC. Thus, the active space appears to be large enough to characterize density changes along the IRC. The peak position of the sum of squares of the singular values indicates that the electron density changes dramatically at the TS. The small change in the sum of squares of the singular values around 4.6 amu$^{1/2}$ bohr in Fig. 10 contributes to strengthening the C–C covalent bonds between ethylene and 1,3-butadiene (Fig. S2 in the supplementary material). Density change to follow the conformational change around the π bond to get planer is also observed.

There is discontinuous behavior of the sum of squares of singular values of MC-NRO in Fig. 10, e.g., at −10.30 amu$^{1/2}$ bohr and around the TS. Such discontinuity originates from discontinuous density matrix change along the IRC. Since the singular values are computed using density matrix derivative evaluated by numerical differentiation, a discontinuity of the density matrix leads to that of the singular values. Also, the discontinuity tends to appear at the ends of IRCs where IRCs often show staggered behavior. However, it must be noted that the nature of active space and MC-NROs does not change discontinuously around these discontinuous points. So, such discontinuity seems not fatal for qualitative analysis of electron transfer during chemical reactions.

The MC-NROs at TS are shown in Fig. 11. The first MC-NRO pair characterizes electron transfer from the C1–C2 and C3–C4 $\pi$ bonds of 1,3-butadiene to the $\pi^*$ orbital of ethylene. The second MC-NRO pair, on the other hand, characterizes electron transfer from the $\pi$ bond of ethylene to the 1,3-butadiene. This result is consistent with our previous study that analyzed the Diels–Alder reaction with NRO at the HF/6-31G(d,p) level.[33] This result is also consistent with the conventional understanding of reaction mechanism based on frontier orbital theory,[60] in which the mutual electron transfer from the highest occupied MO (HOMO)

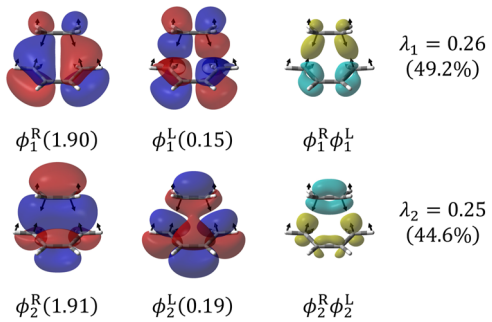


**FIG. 11.** Active–active MC-NRO pairs for the Diels–Alder reaction at TS. $\phi_i^R$ and $\phi_i^L$ represent the $i$-th right and left MC-NROs, and the numbers in parentheses indicate the occupation number. The product of each MC-NRO pair is also shown, with the yellow/cyan color representing the increase/decrease in electron density. $\lambda_i$(amu$^{-1/2}$ bohr$^{-1}$) denotes the singular value of the $i$-th MC-NRO pair. Also shown below each singular value is the contribution of the MC-NRO pair to the overall density change. The isovalues of MC-NRO and density change are 0.020 and 0.004, respectively. The black arrows indicate the motion of the normal vibrational mode with an imaginary frequency from TS toward the product.

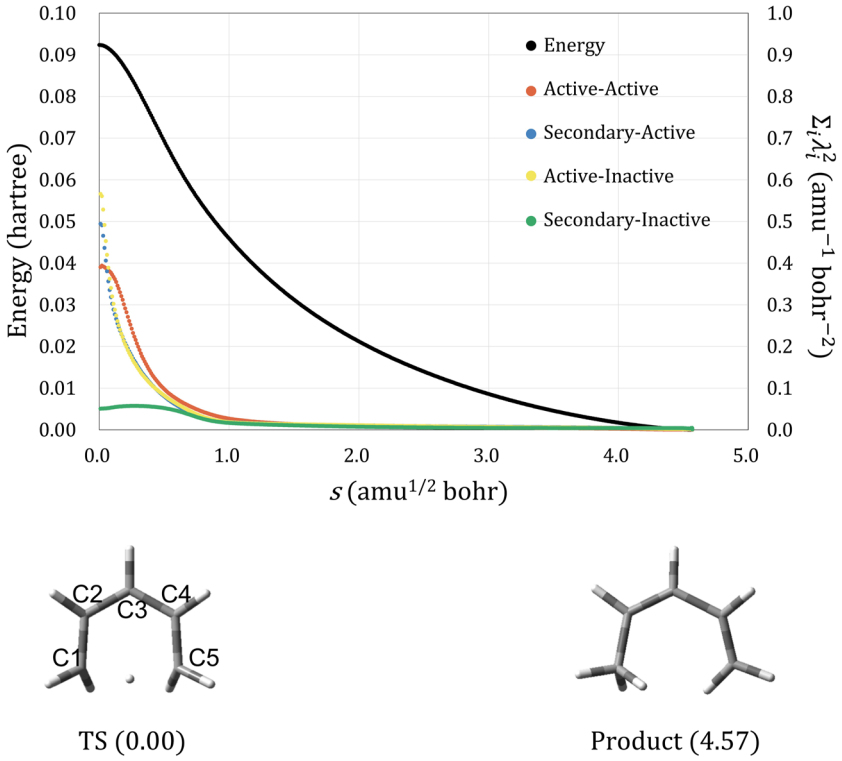


**FIG. 12.** Changes of potential energy along the IRC of the [1,5]-sigmatropic rearrangement of 1,3-pentadiene (black curve), as well as change of the sum of squares of singular values of MC-NROs, denoted by $\sum_i \lambda_i^2$, for the four blocks: active–active (red curve), secondary-active (blue curve), active–inactive (yellow curve), and secondary-inactive (green), at the CASSCF(6,6)/cc-pVTZ level. Geometric structures with reaction coordinates for TS and product (reactant) are shown.

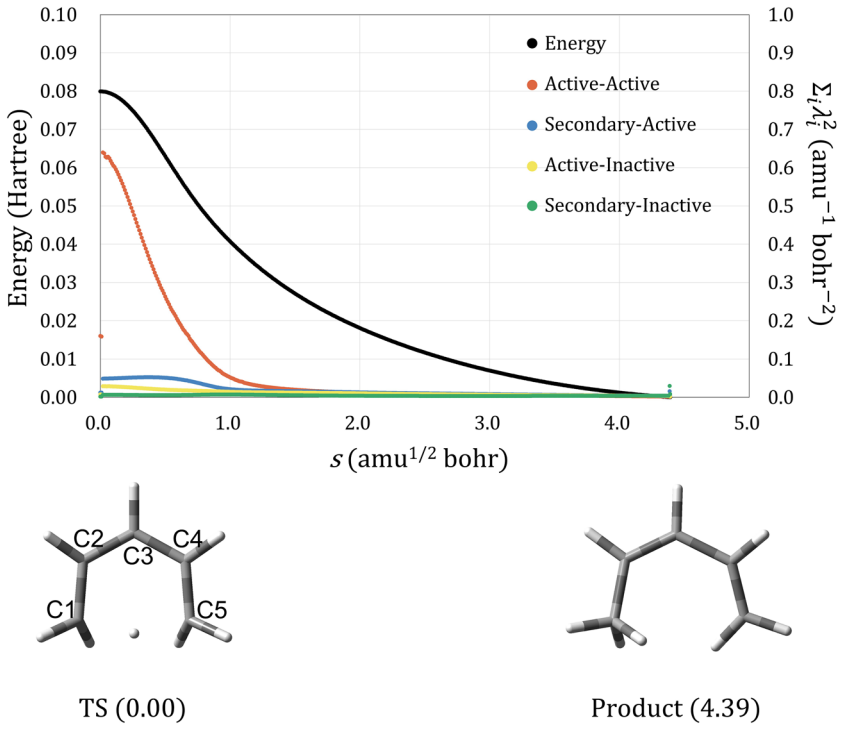


**FIG. 13.** Changes of potential energy along the IRC of the [1,5]-sigmatropic rearrangement of 1,3-pentadiene (black curve), as well as change of the sum of squares of singular values of MC-NROs, denoted by $\sum_i \lambda_i^2$ for four blocks, active–active (red curve), secondary-active (blue curve), active–inactive (yellow curve), and secondary-inactive (green), at the CASSCF(8,8)/cc-pVTZ level. Geometry and reaction coordinates of TS and product (reactant) are shown.

of 1,3-butadiene/ethylene to the lowest unoccupied MO (LUMO) of ethylene/1,3-butadiene drives the Diels–Alder reaction. The density changes shown by MC-NRO clearly characterize the mutual electron transfer. It is also noteworthy that MC-NRO belongs to the irreducible representation of $C_s$ symmetry and, therefore, that chemical reactions can also be analyzed in terms of symmetry based on MC-NRO.

### D. Sigmatropic rearrangement

So far, we have examined examples where symmetry is preserved along the IRC. In the [1,5]-sigmatropic rearrangement of 1,3-pentadiene, the TS has $C_s$ symmetry and falls to $C_1$ symmetry as it proceeds along the IRC. For this reaction, we performed IRC calculations at the CASSCF(6,6)/cc-pVTZ level and performed MC-NRO analysis. Figure 12 shows changes of potential energy and the sum of squares of singular values indicating the degree of electronic density change for four blocks along the IRC. It can be seen that the active space is not large enough to describe the density change because the contribution of the secondary-active and active–inactive blocks is not negligible around the TS.

Considering the above result, the active space was refined by adding one dominant secondary MC-NRO and one dominant inactive MC-NRO to the active space at the TS, and the TS geometry was reoptimized with the improved active space. Figure 13 shows the change in energy and sum of squares of singular values along the IRC at the CASSCF(8,8)/cc-pVTZ level. It can be seen that the quality of the active space can be improved by adding a dominant MC-NRO outside the original active space. Figure 14 shows the energy difference between the CASSCF(6,6) and CASSCF(8,8) results. Note that the IRC is obtained in each active space. The energy difference is relatively large near TS, where MO mixing between active and non-active spaces is observed in Fig. 12. This result suggests that the expansion of the active space with MC-NRO basis effectively improves the quality of the active space. However, this does not necessarily mean that the addition of dominant non-active MC-NRO to the active space always produces good results, since the addition of the MC-NRO may cause problems such as the failure of CASSCF to convergence.

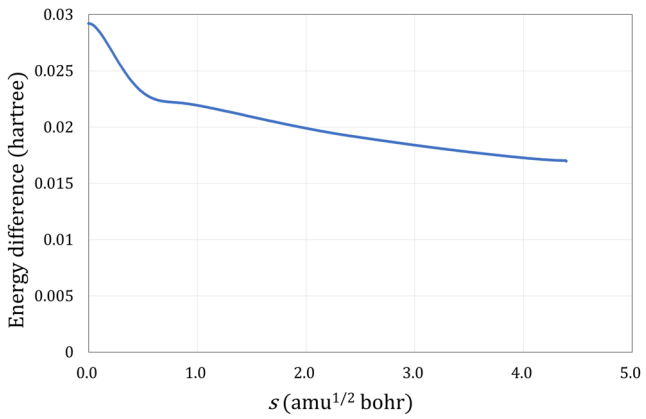


**FIG. 14.** Energy difference between CASSCF(6,6) and CASSCF(8,8) results for the [1,5]-sigmatropic rearrangement of 1,3-pentadiene along the IRC.

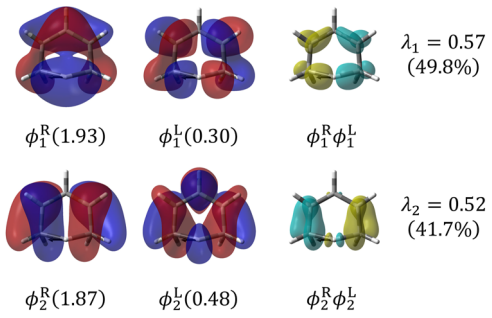


**FIG. 15.** Active–active MC-NRO pairs for the [1,5]-sigmatropic rearrangement at TS. $\phi_i^R$ and $\phi_i^L$ represent the $i$th right and left MC-NROs, and the numbers in parentheses indicate the occupation number. The product of each MC-NRO pair is also shown, with the yellow/cyan color representing the increase/decrease in electron density. $\lambda_i\left(\text{amu}^{-1/2}\,\text{bohr}^{-1}\right)$ denotes the singular values of the $i$th MC-NRO pair. Also shown below each singular value is the contribution of the MC-NRO pair to the overall density change. The isovalues of MC-NRO and density change are 0.020 and 0.004, respectively. The black arrows indicate the normal mode of imaginary frequency directed from TS to the product.

The dominant MC-NROs at TS optimized with extended active space are shown in Fig. 15. The first MC-NRO pair shows a C–H $\sigma$ bond rearrangement with a density increase/decrease in the formed/dissociated C–H bond region. A rearrangement of the $\pi$ bond from C3–C4 to C2–C3 is also observed. The second MC-NRO pair describes a $\pi$ bond rearrangement from C1–C2 to C4–C5. These representative orbitals for reaction, automatically extracted by the MC-NRO method, are consistent with the representative orbitals in the conventional correlation diagram.[61] Thus, the two MC-NRO pairs successfully characterize concerted bonding rearrangements in the [1,5]-sigmatropic rearrangement of 1,3-pentadiene. It was also confirmed that the MC-NRO method works without special problems even when there is symmetry reduction on leaving the TS.

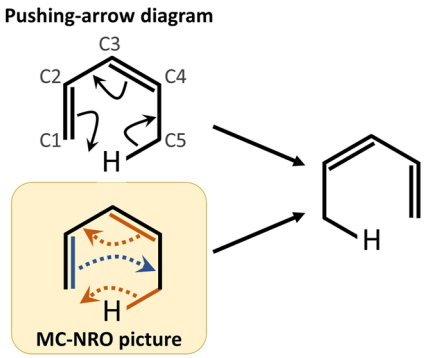


**FIG. 16.** Pushing-arrow diagram and schematic of electron transfer based on MC-NRO analysis of [1,5]-sigmatropic rearrangement of 1,3-pentadiene. The curly arrows of pushing-arrow diagram represent the movement of an electron pair. Note that the dotted arrows in MC-NRO picture just show the direction of electron transfer of the first MC-NRO pair (orange) and the second MC-NRO pair (blue). They do not represent the movement of an electron pair, i.e., they do not indicate the number of electrons.

It should be noted that the electron transfer shown by the MC-NRO method is not consistent with the conventional picture represented by the arrow-pushing diagram (Fig. 16).[61] According to the arrow-pushing diagram, electron transfer occurs from C1–C2 to C1–H, from C3–C4 to C2–C3, and from C5–H to C4–C5. On the other hand, based on the MC-NRO method, electron transfer occurs from C5–H to C1–H, from C3–C4 to C2–C3, and from C1–C2 to C4–C5. The inconsistency is not caused by the symmetry at the TS, and actually electron transfer occurs in the same manner at other geometries along the IRC (Fig. S3 in the supplementary material). Additionally, this kind of inconsistency between the arrow-pushing picture and molecular orbital picture is also seen in Diels–Alder reaction in Subsection III C where the symmetry of the system is preserved ($C_s$ symmetry). For electron transfer analysis based on quantum chemistry calculation, MC-NRO method will be preferable to pushing-arrow method because MC-NRO is obviously consistent with the computational results while pushing-arrow is not necessarily consistent with.

### E. Intramolecular hydrogen transfer of malonaldehyde in the excited state

As a final example, the MC-NRO method is applied to the intramolecular hydrogen transfer of malonaldehyde in the $S_1$ state.[62–66] Excited state reactions are the most important target of MC-NRO analysis, since a multiconfigurational wavefunction is required to describe excited states. The $S_1$ state of malonaldehyde is characterized by a one-electron n-$\pi^*$ excitation.[62–66] Figure 17 shows the natural orbitals related to the excitation to the $S_1$ state obtained with the $S_1$-optimized geometry at the CASSCF(12,9)/cc-pVTZ level. The natural orbitals indicate excitation from the in-plane lone pair of the oxygen atom (hole) to the out-of-plane $\pi^*$ orbital (particle). Figure 18 shows changes of the potential energy and the sum of squares of the singular values along the IRC. The active–active contribution is dominant throughout the IRC, so the active space is large enough to characterize density changes.

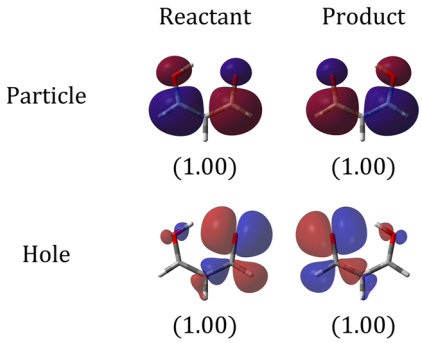


**FIG. 17.** Natural orbitals of malonaldehyde associated with electronic excitation from $S_0$ to $S_1$. The geometry is optimized in the $S_1$ state. Numbers in parentheses indicate the occupation number of each natural orbital.

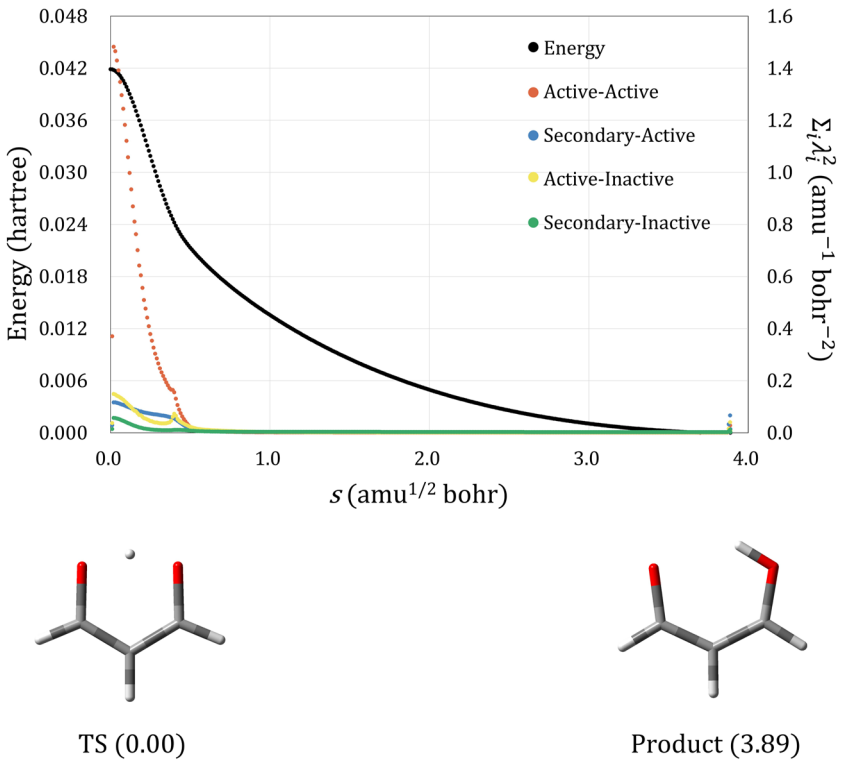


**FIG. 18.** Change of potential energy along the IRC of the hydrogen transfer reaction of malonaldehyde in the $S_1$ state (black curve), as well as change of the sum of squares of singular values of MC-NROs for the four blocks: active–active (red curve), secondary-active (blue curve), active–inactive (yellow curve), and secondary-inactive (green), at the CASSCF(12,9)/cc-pVTZ level. The geometry of TS and product (reactant) is shown with the values of the reaction coordinates.

Figure 19 shows the MC-NROs at TS. The first and second MC-NRO pairs show that the electron is moving in the same direction as the proton migration. This is consistent with the behavior of the hole shown in Fig. 17. As the proton moves from the left oxygen to the right oxygen, the hole center moves from the right oxygen to the left oxygen. Therefore, the electron density moves in the opposite direction of the hole migration, i.e., in the same direction as the proton migration. Since the electron moves with the proton, this reaction should be characterized as hydrogen transfer rather than proton transfer. This is contrary to migration in the ground state, where the electron moves in the opposite direction of proton migration.[33] The $\pi$ density change exhibited by the fourth and fifth MC-NRO pairs is smaller than the density change exhibited by the first and second MC-NRO pairs. This is consistent with the behavior of the particles shown in Fig. 17. The particles are delocalized throughout the molecular plane, and the shape of the particles is hardly changed by hydrogen transfer. Therefore, the change in $\pi$ density is relatively small. As described above, the MC-NRO method can systematically extract representative orbitals for reaction in electronically excited state. Although there are useful orbitals that characterize the nature of excited states, such as natural transition orbitals (NTOs),[67] natural difference orbitals (NDOs),[68] and natural orbitals, the ability to systematically extract representative orbitals for reaction is a feature of MC-NRO. Thus, MC-NRO is expected to be a powerful tool for studying electron mobility in reactions in electronically excited states.

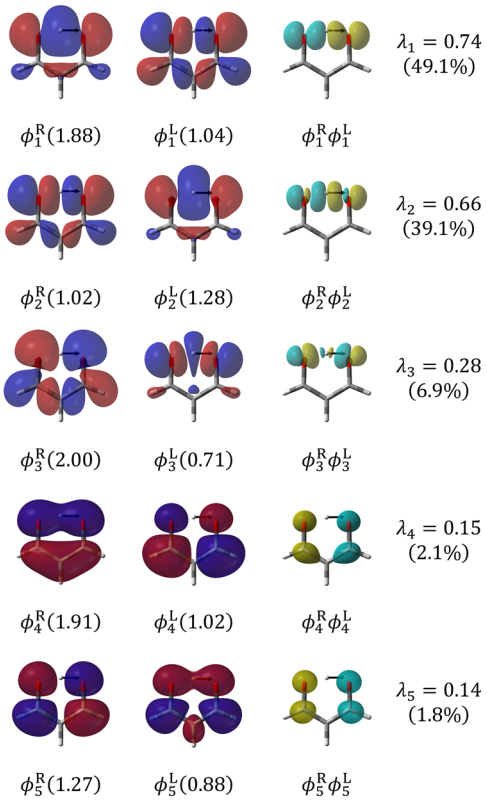


**FIG. 19.** Active–active MC-NRO pairs for hydrogen transfer of malonaldehyde at TS in the $S_1$ state. $\phi_i^R$ and $\phi_i^L$ denote the *i*th right and left MC-NROs, and the numbers in parentheses indicate the occupation number. The product of each MC-NRO pair is also shown, with the yellow/cyan colors representing the increase/decrease in electron density. $\lambda_i\left(\text{amu}^{-1/2}\,\text{bohr}^{-1}\right)$ denotes the singular value of the *i*-th MC-NRO pair. Also shown below each singular value is the contribution of the MC-NRO pair to the overall density change. The isovalues of MC-NRO and density change are 0.020 and 0.004, respectively. The black arrows indicate the normal mode of imaginary frequency from TS toward the product.

## IV. CONCLUSION

In this paper, we extend our recently proposed natural reaction orbital (NRO) to multiconfigurational wavefunction and propose the multiconfiguration natural reaction orbital (MC-NRO), which can reveal the reaction mechanism along the reaction path in terms of electron transfer. In the NRO and MC-NRO methods, pairs of representative orbitals with common singular values are generated by applying SVD to a matrix that characterizes the electron density change due to the displacement of nuclear coordinates. The importance in the reaction of the electron transfer represented by each representative orbital pair can be evaluated by the magnitude of the singular value. By taking the product of each representative orbital pair, the change in electron density for a given nuclear coordinate displacement can be visualized. Since the MC-NRO method by definition does not violate orbital invariance, the properties of each MC-NRO other than density change can be analyzed without suffering from contributions from outside the variational manifold. In addition, MC-NRO belongs to an irreducible representation of the point group of the molecular structure. The MC-NRO method is based on multiconfigurational wavefunction theory and is expected to be a practical tool for extracting the qualitative essence of a wider range of chemical reactions, such as covalent bond dissociation and chemical reactions in electronically excited states.

The most important advantage of the MC-NRO method is its ability to automatically extract representative orbitals for a given chemical reaction without requiring in-depth knowledge of the chemical reaction. In particular, the systematic identification of representative orbitals for a given reaction in the electronically excited state is very useful for studying reactions in excited states that are more complex than those in the ground state. It is also shown that the MC-NRO method can be used to verify the descriptive performance of the active space of the CASSCF wavefunction in reaction processes. Using the MC-NRO method, not only the change in electron density due to orbital mixing but also the change in CI coefficients can be characterized in terms of MOs. Visualization of complex CI coefficients by MOs is very useful for analyzing electron mobility and is expected to enhance our understanding of various chemical phenomena in electronically excited states.

## SUPPLEMENTARY MATERIAL

See the supplementary material for more information on the following: S1 for a compact explanation for the matrix of Eq. (16) in II C; S2 for procedure to compute MC-NRO for the electronic structure theories other than CASSCF; S3 for properties of MC-NRO, symmetry, and behavior with regard to orbital rotation;

S4 for natural orbitals in the active space of hydrogen molecule at CASSCF(2,10)/aug-cc-pVQZ level (III A); S5 for MC-NRO of Diels–Alder reaction at $s = 4.59$ amu$^{1/2}$ bohr in Fig. 10 (III C); and S6 for MC-NRO of [1,5]-sigmatropic rearrangement at $s = 0.50$ amu$^{1/2}$ bohr (III D).

## ACKNOWLEDGMENT

S.E. acknowledges the support from the Institute for Quantum Chemical Exploration through the Research Fellowship for Young Scientists, the MEXT Doctoral program for DataRelated InnoVation Expert Hokkaido University (D-DRIVE-HU), and the Hokkaido University DX Doctoral Fellowship of MEXT (Grant No. JPMJSP2119). This work was also partly supported by the Photo-excitonix Project at Hokkaido University and JST CREST, Japan (Grant No. JPMJCR1902). A part of calculations was performed using the Research Center for Computational Science, Okazaki, Japan (Project No.: 22-IMS-C019).

## AUTHOR DECLARATIONS

### Conflict of Interest

The authors have no conflicts to disclose.

### Author Contributions

**Shuichi Ebisawa**: Conceptualization (lead); Data curation (lead); Formal analysis (lead); Investigation (lead); Methodology (lead); Software (equal); Validation (lead); Writing – original draft (lead). **Takuro Tsutsumi**: Conceptualization (equal); Investigation (equal); Writing – review & editing (equal). **Tetsuya Taketsugu**: Conceptualization (equal); Funding acquisition (lead); Investigation (equal); Methodology (equal); Project administration (equal); Writing – review & editing (equal).

## DATA AVAILABILITY

The data that support the findings of this study are available within the article and its supplementary material.

## REFERENCES

[1] F. Hund, Z. Physik **51**, 759 (1928).
[2] R. S. Mulliken, Phys. Rev. **32**, 186 (1928).
[3] K. Fukui, T. Yonezawa, and H. Shingu, J. Chem. Phys. **20**, 722 (1952).
[4] K. Fukui, T. Yonezawa, and C. Nagata, Bull. Chem. Soc. Jpn. **27**, 423 (1954).
[5] R. B. Woodward and R. Hoffmann, J. Am. Chem. Soc. **87**, 395 (1965).
[6] R. Hoffmann and R. B. Woodward, J. Am. Chem. Soc. **87**, 2046 (1965).
[7] R. Hoffmann and R. B. Woodward, J. Am. Chem. Soc. **87**, 4388 (1965).
[8] R. B. Woodward and R. Hoffmann, Angew. Chem., Int. Ed. **8**, 781 (1969).
[9] R. Hoffmann and R. B. Woodward, Science **167**, 825 (1970).
[10] G. Montavon, M. Rupp, V. Gobre, A. Vazquez-Mayagoitia, K. Hansen, A. Tkatchenko, K.-R. Müller, and O. Anatole von Lilienfeld, New J. Phys. **15**, 095003 (2013).
[11] O. A. von Lilienfeld, K.-R. Müller, and A. Tkatchenko, Nat. Rev. Chem. **4**, 347 (2020).
[12] H. Jónsson, G. Mills, and K. W. Jacobsen, "Nudged elastic band method for finding minimum energy paths of transitions," in *Classical and Quantum Dynamics in Condensed Phase Simulations*, edited by B. J. Berne, G. Ciccotti, and D. F. Coker (World Scientific, Singapore, 1998), Chap. 16, pp. 385–404.
[13] W. Quapp, M. Hirsch, O. Imig, and D. Heidrich, J. Comput. Chem. **19**, 1087 (1998).
[14] K. Ohno and S. Maeda, Chem. Phys. Lett. **384**, 277 (2004).
[15] S. Maeda and K. Ohno, J. Phys. Chem. A **109**, 5724 (2005).
[16] S. Maeda and K. Morokuma, J. Chem. Phys. **132**, 241102 (2010).
[17] M. Shoji, M. Kayanuma, and Y. Shigeta, Bull. Chem. Soc. Jpn. **91**, 1465 (2018).
[18] K. Fukui, J. Phys. Chem. **74**, 4161 (1970).
[19] V. Fock, Z. Physik **61**, 126 (1930).
[20] T. Tsutsumi, Y. Ono, Z. Arai, and T. Taketsugu, J. Chem. Theory Comput. **14**, 4263 (2018).
[21] T. Tsutsumi, Y. Ono, Z. Arai, and T. Taketsugu, J. Chem. Theory Comput. **16**, 4029 (2020).
[22] S. R. Hare, L. A. Bratholm, D. R. Glowacki, and B. K. Carpenter, Chem. Sci. **10**, 9954 (2019).
[23] A. I. Krylov, J. Chem. Phys. **153**, 080901 (2020).
[24] P. O. Löwdin, Phys. Rev. **97**, 1474 (1955).
[25] C. Edmiston and K. Ruedenberg, Rev. Mod. Phys. **35**, 457 (1963).
[26] K. Fukui, N. Koga, and H. Fujimoto, J. Am. Chem. Soc. **103**, 196 (1981).
[27] A. E. Reed and F. Weinhold, J. Chem. Phys. **78**, 4066 (1983).
[28] A. E. Reed and F. Weinhold, J. Chem. Phys. **83**, 1736 (1985).
[29] G. Knizia, J. Chem. Theory Comput. **9**, 4834 (2013).
[30] M. W. Schmidt, E. A. Hull, and T. L. Windus, J. Phys. Chem. A **119**, 10408 (2015).
[31] J.-X. Zhang, F. K. Sheong, and Z. Lin, Chem. - Eur. J. **24**, 9639 (2018).
[32] K. Takatsuka and Y. Arasaki, J. Chem. Phys. **154**, 094103 (2021).
[33] S. Ebisawa, M. Hasebe, T. Tsutsumi, T. Tsuneda, and T. Taketsugu, Phys. Chem. Chem. Phys. **24**, 3532 (2022).
[34] K. Ruedenberg, M. W. Schmidt, M. M. Gilbert, and S. T. Elbert, Chem. Phys. **71**, 41 (1982).
[35] K. Ruedenberg, M. W. Schmidt, and M. M. Gilbert, Chem. Phys. **71**, 51 (1982).
[36] A. T. Amos and G. G. Hall, Proc. Roy. Soc. **A263**, 483 (1961).
[37] R. McWeeny, Rev. Mod. Phys. **32**, 335 (1960).
[38] J. Gerratt and I. M. Mills, J. Chem. Phys. **49**, 1719 (1968).
[39] J. A. Pople, R. Krishnan, H. B. Schlegel, and J. S. Binkley, Int. J. Quantum Chem. **16**, 225 (1979).
[40] A. Morita and S. Kato, J. Am. Chem. Soc. **119**, 4021 (1997).
[41] J. A. Pople, R. Seeger, and R. Krishnan, Int. J. Quantun Chem. **12**, 149 (1977).
[42] B. O. Roos, P. R. Taylor, and P. E. M. Sigbahn, Chem. Phys. **48**, 157 (1980).
[43] A. D. McLachlan and M. A. Ball, Rev. Mod. Phys. **36**, 844 (1964).
[44] R. Bauernschmitt and R. Ahlrichs, Chem. Phys. Lett. **256**, 454 (1996).
[45] M. E. Casida, C. Jamorski, K. C. Casida, and D. R. Salahub, J. Chem. Phys. **108**, 4439 (1998).
[46] P. Lancaster and M. Tismenetsky, *The Theory of Matrices*, 2nd ed (Academic Press, London, 1985).
[47] L. Hogben, *Handbook of Linear Algebra*, 2nd ed (Chapman and Hall/CRC, Boca Raton, Florida, 2013).
[48] H. J. Werner and W. Meyer, J. Chem. Phys. **74**, 5794 (1981).
[49] L. N. Tran and E. Neuscamman, J. Phys. Chem. A **124**, 8273 (2020).
[50] L. Kong, Int. J. Quantum Chem. **110**, 2603 (2010).
[51] M. J. Frisch, G. W. Trucks, H. B. Schlegel, G. E. Scuseria, M. A. Robb, J. R. Cheeseman, G. Scalmani, V. Barone, G. A. Petersson, H. Nakatsuji, X. Li, M. Caricato, A. V. Marenich, J. Bloino, B. G. Janesko, R. Gomperts, B. Mennucci, H. P. Hratchian, J. V. Ortiz, A. F. Izmaylov, J. L. Sonnenberg, D. Williams-Young, F. Ding, F. Lipparini, F. Egidi, J. Goings, B. Peng, A. Petrone, T. Henderson, D. Ranasinghe, V. G. Zakrzewski, J. Gao, N. Rega, G. Zheng, W. Liang, M. Hada, M. Ehara, K. Toyota, R. Fukuda, J. Hasegawa, M. Ishida, T. Nakajima, Y. Honda, O. Kitao, H. Nakai, T. Vreven, K. Throssell, J. A. Montgomery, Jr., J. E. Peralta, F. Ogliaro, M. J. Bearpark, J. J. Heyd, E. N. Brothers, K. N. Kudin, V. N. Staroverov, T. A. Keith, R. Kobayashi, J. Normand, K. Raghavachari, A. P. Rendell, J. C. Burant, S. S. Iyengar, J. Tomasi, M. Cossi, J. M. Millam, M. Klene, C. Adamo, R. Cammi, J. W. Ochterski, R. L. Martin, K. Morokuma, O. Farkas, J. B. Foresman, and D. J. Fox, GAUSSIAN 16, Revision C.01, Gaussian, Inc., Wallingford CT, 2016.

[52]A. D. McLean, A. Weiss, and M. Yoshimine, Rev. Mod. Phys. **32**, 211 (1960).
[53]G. Das and A. C. Wahl, J. Chem. Phys. **44**, 87 (1966).
[54]T. H. Dunning, Jr., J. Chem. Phys. **90**, 1007 (1989).
[55]R. A. Kendall, T. H. Dunning, Jr., and R. J. Harrison, J. Chem. Phys. **96**, 6796 (1992).
[56]A. Szabo and N. S. Ostlund, *Modern Quantum Chemistry: Introduction to Advanced Electronic Structure Theory* (McGraw-Hill, New York, 1989).
[57]B. H. Botch and T. H. Dunning, Jr., J. Chem. Phys. **76**, 6046 (1982).
[58]S. P. Walch, J. Chem. Phys. **86**, 5670 (1987).
[59]C. W. Bauschlicher, Jr., S. P. Walch, S. R. Langhoff, P. R. Taylor, and R. L. Jaffe, J. Chem. Phys. **88**, 1743 (1988).
[60]K. Fukui, Science **218**, 747 (1982).
[61]H. Nohira and T. Nohira, J. Theor. Comput. Chem. **16**, 1750055 (2017).
[62]A. L. Sobolewski and W. Domcke, J. Chem. Phys. **103**, 4494 (1999).
[63]T. Kar, S. Scheiner, and M. Čuma, J. Chem. Phys. **111**, 849 (1999).
[64]J. D. Coe and T. J. Martínez, J. Phys. Chem. A **110**, 618 (2006).
[65]K. R. Nandipati, A. K. Kanakati, H. Singh, and S. Mahapatra, Phys. Chem. Chem. Phys. **21**, 20018 (2019).
[66]N. H. List, A. L. Dempwolff, A. Dreuw, P. Norman, and T. J. Martínez, Chem. Sci. **11**, 4180 (2020).
[67]R. L. Martin, J. Chem. Phys. **118**, 4775 (2003).
[68]F. Plasser, M. Wormit, and A. Dreuw, J. Chem. Phys. **141**, 024106 (2014).